MARTHINSEN, K. & HØIER, R. (1988*b*). *Acta Cryst.* A**44**, 700-707.
PIROUZ, P. (1974). *Z. Naturforsch. Teil A*, **29**, 1188-1197.
SCHULSON, E. M. (1977). *J. Mater. Sci.* **12**, 1071-1087.
SPENCER, J. P., HUMPHREYS, C. J. & HIRSCH, P. B. (1972). *Philos. Mag.* **26**, 193-213.
STEEDS, J. W. & VINCENT, R. (1983). *J. Appl. Cryst.* **16**, 317-324.
TANAKA, M., SEKII, H. & NAGASAWA, T. (1983). *Acta Cryst.* A**39**, 825-837.
WALKER, A. R. & BOOKER, G. R. (1982). *Electron Microsc.* **1**, 651-652.

Acta Cryst. (1988). A**44**, 700-707

On the Breakdown of Friedel's Law in Electron Backscattering Channelling Patterns

BY KNUT MARTHINSEN* AND RAGNVALD HØIER

Department of Physics and Mathematics, University of Trondheim-NTH, N-7034 Trondheim, Norway

(*Received* 1 *February* 1988; *accepted* 14 *April* 1988)

Abstract

The theory for electron channelling patterns has been investigated. Calculations based on existing intensity expressions have been found inadequate for explaining recently observed deviations from Friedel's law. This is found to be the case even if the calculations are based on the full non-Hermitian eigenvalue matrix. The theory has hence been reinvestigated and a new intensity expression has been derived which includes the inter Bloch-wave coupling terms and is valid for non-centrosymmetric polyatomic crystals. The expression explains the observed asymmetries for GaSb which make it possible to determine unambiguously the correct non-centrosymmetric point group for this crystal. It is further found that the same effects in GaAs should be very weak in accordance with the non-observed deviation from Friedel's law in this case.

Introduction

Violation of Friedel's law in electron diffraction experiments is due to dynamical interactions between simultaneously excited Bragg beams (*e.g.* Kohra, 1954; Miyake & Uyeda, 1955; Fujimoto, 1959). Asymmetries which could be ascribed to this effect were reported for the non-centrosymmetric structure of ZnS by Thiessen & Molière (1939) and also by Miyake & Uyeda (1950). More recently, convergent-beam electron diffraction (CBED) and the bend extinction contour technique have proved to be well suited to reveal deviations from Friedel's law and consequently the absence of a centre of symmetry in a non-centrosymmetric structure (*e.g.* Goodman & Lehmpfuhl, 1968; Steeds, Tatlock & Hampson, 1973; Goodman, 1975; Steeds & Vincent, 1983).

In selected area channelling patterns (SACP), however, deviations from centrosymmetry have not been observed until recently. In a general investigation of the possible use of the SACP technique in structure studies (Høier & Marthinsen, 1986; Marthinsen, 1986; Marthinsen & Høier, 1988), effects have been observed for gallium antimonide which make it possible to determine the correct non-centrosymmetric point group in this case. Such effects, which may be ascribed to the failure of Friedel's law in electron channelling patterns, cannot be explained by any of the existing theoretical expressions as given, for example, by Reimer, Badde, Seidel & Bühring (1971), Spencer, Humphreys & Hirsch (1972), Yamamoto, Mori & Ishida (1978) or Spencer & Humphreys (1980).

The aim of the present work has been to investigate these observed effects more thoroughly. The theory is hence reinvestigated in order to obtain an expression which is able to account for the observations from gallium antimonide. As is well known from CBED, for example, the possible identification of a non-centrosymmetric structure is coupled to the interaction terms between the different Bloch waves. On this basis it may therefore be assumed that a many-beam intensity expression for channelling patterns has also to include these coupling terms. Their contribution to the channelling contrast from GaSb and GaAs is investigated in particular both theoretically and experimentally. Some preliminary results have been given previously (Marthinsen & Høier 1986*a*; Marthinsen, Anisdahl & Høier, 1987).

Experimental

The experiments were carried out in a JSM-840 scanning electron microscope. All the patterns reproduced below were obtained near a ⟨001⟩ zone.

*Present address: SINTEF, Division of Applied Physics, N-7034 Trondheim, Norway.

0108-7673/88/050700-08$03.00

A reproduction of a [001] zone-axis pattern from GaSb is shown in Fig. 1(*a*). The interesting asymmetry is most clearly seen in the ⟨105⟩ zones. Lines to be compared are indicated by arrows. It is seen that mirror symmetry is violated across the 200 bands but retained across the 220 bands. For the ⟨001⟩ full pattern symmetry $2mm$ results, and this is in accordance with the point group of GaSb ($\bar{4}3m$). Details from the [105] zone are shown in Fig. 1(*b*). The most important lines involved in the asymmetry are given schematically in Fig. 3. The most prominent features are shown by heavy lines. In the upper part the $53\bar{1}$ line contrast is seen to dominate between the 040 and 020 lines while the $5\bar{1}\bar{1}$ line contrast seems to dominate the whole length between the 020 and $0\bar{4}0$ lines. Between the $0\bar{2}0$ and the $0\bar{4}0$ line the $5\bar{3}\bar{1}$ line is also observed, but less marked than the $53\bar{1}$ line in the symmetrical position. In the lower part the $\bar{5}31$ line has a strong segment between the 020 and the 040 line while $\bar{5}\bar{1}1$ dominates between the 020 and $0\bar{4}0$ lines. The difference in contrast between the $51\bar{1}$ and $5\bar{1}\bar{1}$ lines at symmetrical positions about the band center may be considered as a violation of Friedel's law in a broad sense since the $5\bar{1}\bar{1}$ reflection is equivalent to the $\bar{5}\bar{1}1$ reflection in GaSb, and because this effect makes it possible to determine the correct non-centrosymmetric point group in this case.

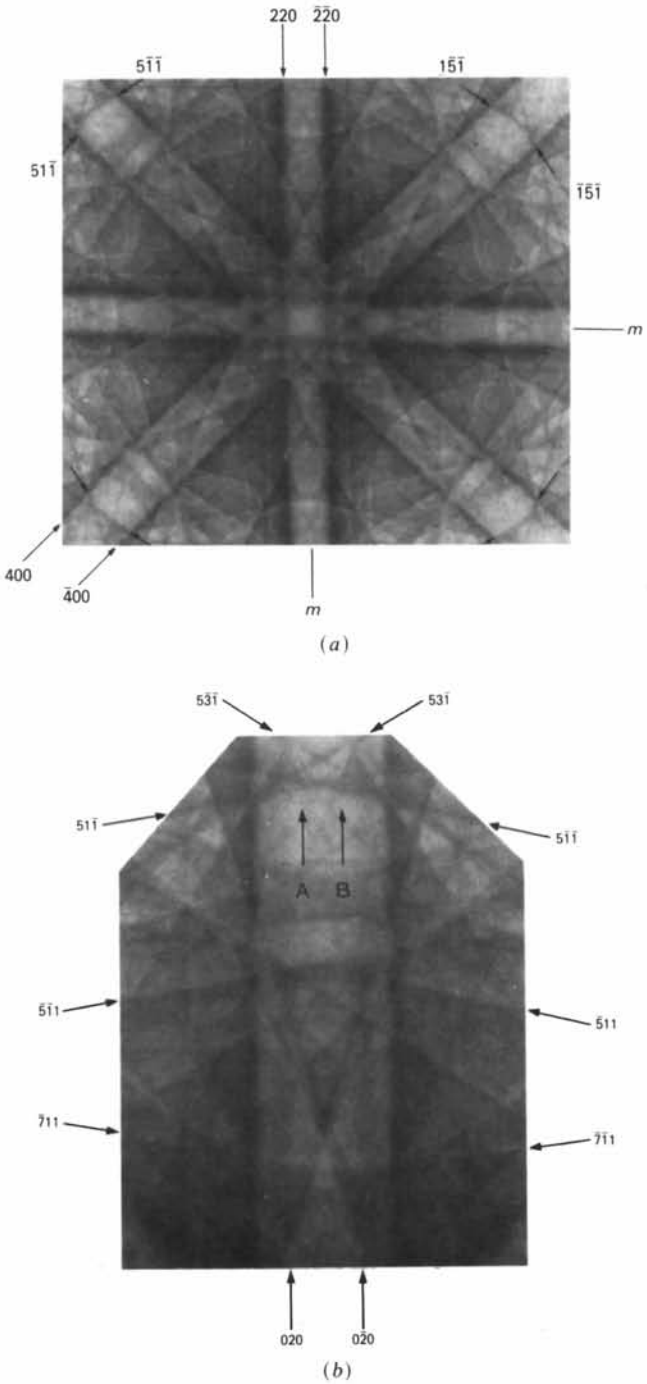

Fig. 1. (*a*) SACP near the [001] zone in GaSb. Arrows show lines with asymmetric contrast in the ⟨105⟩ zones. (*b*) Details from the [105] zone. The sections *A* and *B* indicate the positions of the contrast profiles given in Fig. 6.

A similar asymmetry to the one discussed above is also observed in the $\bar{7}11$ and $\bar{7}\bar{1}1$ lines belonging to the [107] zone in Fig. 1(*b*).

We have also looked for similar effects in GaAs which has the same point group and space group as GaSb (point group $\bar{4}3m$; space group $F\bar{4}3m$). There is, however, a very important distinction between the two crystals. Owing to the large difference in atomic number between Ga and Sb, GaSb deviates strongly from centrosymmetry. GaAs, on the other hand, deviates very little from centrosymmetry. A close-up view of the [105] zone-axis pattern from GaAs is shown in Fig. 2. No asymmetry like the one observed for GaSb is observed in the prominent lines. As explained by Marthinsen & Høier (1988) one may for this reason erroneously be led to the conclusion that the [001] zone-axis pattern of GaAs has $4mm$ symmetry.

Theory

As with several previous theories for electron channelling contrast, we shall consider the incident electrons in the crystal as a superposition of Bloch waves (*e.g.* Reimer, Badde, Seidel & Bühring, 1971; Spencer, Humphreys & Hirsch, 1972). It is further assumed that the main mechanism responsible for backscattering is phonon scattering. One of the present authors has recently performed a generalization of the expressions of Spencer *et al.* (1972) to include polyatomic crystals (Marthinsen, 1986). We shall follow the same procedure as outlined in that work to obtain an analytical expression for the thermal diffuse scattering. In the present derivation, however, the coupling terms between the different Bloch waves are also included, *i.e.* the Bloch waves are no longer assumed to backscatter independently.

Consider a crystal of thickness t with a slice of thickness dz at depth z with dz/V_c unit cells per unit area (V_c = the unit-cell volume). In the upper part of the crystal (above dz) the incident beam, $\mathbf{k}_0$, is Bragg scattered into discrete beams $\mathbf{g}$ with a strength given by the scattering-matrix elements

$$S_{g0}(\mathbf{k}_0, z) = \sum_i C_0^{i*} C_g^i \, e^{i\gamma^i z} \tag{1}$$

where C_g^i is a component of the ith Bloch-wave eigenvector $|C^i\rangle$ corresponding to the eigenvalue γ^i. C_0^{i*} is the excitation coefficient of the ith Bloch wave and follows from the boundary condition of continuity of the electron wave function at the top crystal surface (*e.g.* Humphreys, 1979).

In the slice dz kinematical thermal diffuse scattering takes place from all the Bragg beams into the direction $\mathbf{s}$. Following the procedure of Marthinsen (1986), which is a generalization of the two-beam theory of Hall & Hirsch (1965), and in addition including the coupling terms between the different Bloch waves, one obtains for the thermal diffuse scattering in dz

$$dI_D(\mathbf{s}, z) = (dz/V_c) \sum_i \sum_j C_0^{i*} C_0^j \exp[i(\gamma^i - \gamma^j)z] \times \exp[-(\mu^i + \mu^j)z] \sum_g \sum_h C_g^i C_h^{j*} \times \sum_J f_{s-g}^J f_{s-h}^{J*} \times [\exp(-M_{h-g}^J) - \exp(-M_{s-g}^J - M_{s-h}^J)] \times \exp[i(\mathbf{h}-\mathbf{g}) \cdot \mathbf{r}_J]. \tag{2}$$

Here μ^i is the Bloch-wave amplitude absorption coefficient. f_{s-g}^J is an atomic scattering amplitude for atom J, and $\exp(-M_{h-g}^J)$ is the Debye–Waller factor associated with atom J for the reflection $(\mathbf{h}-\mathbf{g})$. The summation over J is taken over the atoms at positions $\mathbf{r}_J$ in the unit cell.

For large values of $\mathbf{s}$ corresponding to backscattering we can make the following simplification in (2) (*cf.* Spencer *et al.*, 1972). Since $|s| \gg |g|$ and $|h|$,

$$\exp(-M_{s-g}^J) \simeq \exp(-M_{s-h}^J) \simeq 0.$$

Moreover, $f_{s-h}^J \simeq f_{s-g}^J \simeq f_s^J$, and f_s^J is to a good approximation given by the Rutherford part of the scattering factor, *i.e.*

$$|f_s^J|^2 = (e^2 m Z_J / 4\pi\varepsilon_0 h^2)^2 (4\pi)^4 / 4s^4. \tag{3}$$

Here Z_J is the atomic number, and e and m are the charge and mass of the electron, respectively. $s = 4\pi(\sin\theta)/\lambda$ where λ is the wavelength of the electron. h is Planck's constant and ε_0 is the permittivity of free space. To obtain the backscattered intensity dI_B from dz, we need to find the fraction of electrons which is scattered into directions towards the surface of the crystal. This implies that $dI_D(\mathbf{s}, z)$ must be integrated over all values of $\mathbf{s}$ corresponding to backscattering. Assuming normal incidence and employing the simplifications made above, one gets after integration

$$dI_B(z) = \frac{dz}{V_c} \pi \left(\frac{e^2 m \lambda^2}{4\pi\varepsilon_0 h^2}\right)^2 \sum_i \sum_j C_0^{i*} C_0^j \times \exp[i(\gamma^i - \gamma^j)z] \times \exp[-(\mu^i + \mu^j)z] \sum_g \sum_h C_g^i C_h^{j*} \sum_J Z_J^2 \times \exp(-M_{h-g}^J) \exp[i(\mathbf{h}-\mathbf{g}) \cdot \mathbf{r}_J]. \tag{4}$$

To get the total intensity backscattered from the crystal, (4) must be integrated over all thicknesses t. Redistribution of the electrons on their way out of the crystal is ignored as the dominating amount will still be in the backscattering hemisphere and hence will reach the detector.

We have to evaluate the integral

$$I = \int_0^t \exp[i(\gamma^i - \gamma^j)z] \exp[-(\mu^i + \mu^j)z] \, dz. \tag{5}$$

For bulk crystals we may safely take the upper integration limit to be $t = \infty$. Then the integral may be evaluated to give (Gradshteyn & Ryzhik, 1980)

$$I = [(\mu^i + \mu^j) + i(\gamma^i - \gamma^j)]/[(\gamma^i - \gamma^j)^2 + (\mu^i + \mu^j)^2]. \tag{6}$$

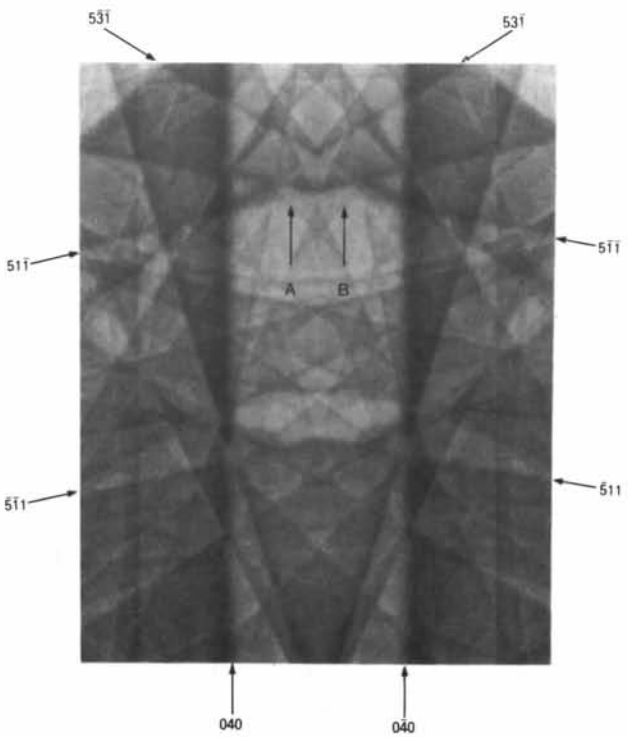

Fig. 2. SACP near the [105] zone in GaAs. Apparently mirror symmetry in the 020 band. The sections *A* and *B* indicate the positions of the contrast profiles given in Fig. 8.

Using (6) we may finally obtain for the total backscattered intensity I_B the expression

$$I_B = \frac{\pi}{V_c}\left(\frac{e^2 m\lambda^2}{4\pi\varepsilon_0 h^2}\right)^2 \sum_i \sum_j |A^{ij}| \times \frac{(\mu^i+\mu^j)\cos\Phi_{ij} - (\gamma^i-\gamma^j)\sin\Phi_{ij}}{(\gamma^i-\gamma^j)^2+(\mu^i+\mu^j)^2} \quad (7)$$

where

$$A^{ij} = C_0^{i*} C_0^j \sum_g \sum_h C_g^i C_h^{j*} \times \sum_J Z_J^2 \exp(-M_{h-g}^J) \exp[i(\mathbf{h}-\mathbf{g})\cdot\mathbf{r}_J] \quad (8)$$

and Φ_{ij} is the phase of A^{ij}. The Bloch-wave eigenvector components, C_g^i, and the eigenvalues γ^i defining the dispersion surface may be found from the eigenvalue equation of standard many-beam electron diffraction theory (*e.g.* Humphreys, 1979),

$$\mathbf{M}|C^i\rangle = 2k\gamma^i|C^i\rangle \quad (9)$$

where $M_{00}=0$, $M_{gg}=2ks_g$, $M_{hg}=U_{h-g}$.

Here s_g is the excitation error for the diffracted beam g, and U_{h-g} is a Fourier coefficient of the real part of the potential $U(\mathbf{r})$. When $U(\mathbf{r})$ is real, $U_g = U^*_{-g}$ and the matrix $\mathbf{M}$ is Hermitian. Hence the eigenvalues γ^i are real although the eigenvectors C_g^i are, in general, complex. The eigenvectors, however, will form a complete orthonormal set. Absorption is formally introduced by the addition of an imaginary part $iU'(\mathbf{r})$ to the potential. This part is normally treated as a small perturbation and the Bloch-wave amplitude absorption coefficients are calculated from the perturbation expression

$$2k\mu^i = U_0' + \sum_{h\neq g}\sum U'_{h-g} C_h^{i*} C_g^i, \quad (10)$$

where k is the wave vector and U'_{h-g} is a Fourier coefficient of the imaginary part of the crystal potential. To estimate these Fourier coefficients it is assumed that the non-Hermitian part of the potential has the same dependence on position as the real part, and we have used the approximation

$$(\text{Re } U_h')/(\text{Re } U_n) \simeq (\text{Im } U_h')/(\text{Im } U_h) \simeq 0{\cdot}1. \quad (11)$$

Although it may be quantitatively inaccurate, we still believe that such an approximation takes care of the typical variations in μ^i [(10)] with the diffraction condition. The Fourier coefficients of the Hermitian part of the potential are all calculated from Doyle & Turner (1968).

In (8) a Debye-Waller factor for each atomic type is included. However, in the calculations we have for simplicity assumed a common Debye-Waller factor, and the Debye-Waller factors for the compounds in question are used. The temperature factors B for GaSb and GaAs are taken from *International Tables for X-ray Crystallography* (1962).

The many-beam intensity expression in (7) is generally valid for polyatomic and non-centrosymmetric crystals. The theory of Reimer *et al.* (1971) did also include the coupling terms, ij, between the different Bloch waves, but their formulation is not valid for general non-centrosymmetric and polyatomic crystals. It should be noted that in the derivation of (7) we have not taken into account effects of multiple inelastic scattering. The background contrast level is therefore not correct. However, the intensity expression (7) includes all the essential Bragg scattering effects and is thus expected to be well suited for qualitative comparisons between calculated diffraction effects and experiments.

Calculations and discussions

All the calculations presented below refer to the line pattern shown schematically in Fig. 3. To solve the dynamical eigenvalue equation [(9)] for the diffraction conditions in question, *i.e.* to determine the Bloch-wave amplitudes C_g^i and the corresponding *Anpassungen* γ^i, we have utilized a software routine which is based on a diagonalization algorithm described by Peters & Wilkinson (1970) (see also Wilkinson & Reinsch, 1971). This routine is able to handle Hermitian as well as non-Hermitian matrices.

From standard SACP theory the contrast profiles along the symmetrical sections A and B in Fig. 3

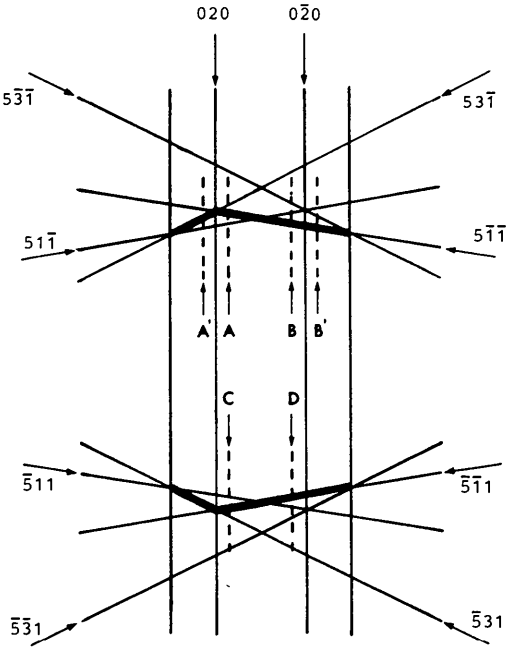

Fig. 3. A schematic drawing of the intensity anomalies in Fig. 1, [105] zone. The sections A, A', B and B' indicate the positions of the contrast profiles given in Fig. 6.

should be identical. In Fig. 4(*a*) a cut through the dispersion surface for section *A* in GaSb is shown. Five beams (*viz* 000, 020, $5\bar{1}\bar{1}$, $51\bar{1}$ and $53\bar{1}$) are taken into account in these calculations. The same dispersion surface is valid for section *B* if the five corresponding beams are taken into account. This follows from the fact that the eigenvalue matrices **M** for the sections *A* and *B* are then related by $\mathbf{M}_A = \mathbf{M}_B^T = \mathbf{M}_B^*$ (the second equality follows from the Hermitian property of **M** when absorption is excluded). If the contrast profiles along the sections *A* and *B* are calculated from (7), without the coupling terms, *ij*, between the different Bloch waves, the same profiles result (Fig. 4*b*), giving a mirror plane in the middle of the 020 band. It should be noted that (7) without the coupling terms, *ij*, is (apart from a background term) almost equivalent to the intensity expression of Spencer *et al.* (1972). This expression therefore leads to the same conclusions as above. However, as pointed out previously, the mirror plane in the middle of the 020 band is neither observed nor in accordance with the structure.

In a first attempt to explain the observed effects from GaSb, the coupling terms between the different Bloch waves were still ignored. But instead of taking into account absorption by perturbation theory, the imaginary part of the potential was introduced in the original dynamical equations, and the resulting non-Hermitian eigenvalue problem (9) was solved for the sections *A* and *B*. A slightly modified version of (7) without the coupling terms, *ij*, was used to calculate the contrast profiles. The modifications are discussed in the Appendix and the resulting calculations are shown in Fig. 5. We notice that there are only minor differences between the two profiles, and the asymmetry is far too small to account for the experimental observations of GaSb.

The reason why there are differences at all is that the eigenvalue matrices for the two sections are different ($\mathbf{M}_A = \mathbf{M}_B^T \neq \mathbf{M}_B^*$), giving slightly different eigenvector sets. Comparison with Fig. 4(*b*) shows further that the effect of diagonalizing the full complex eigenvalue matrix is small. It may be concluded from these results that including absorption through a non-Hermitian matrix is not sufficient to explain the asymmetry observed in the electron channelling patterns (Fig. 1) from GaSb.

We therefore proceeded to the investigation of the influence of the coupling terms between the different Bloch waves. In all the subsequent calculations absorption is treated by perturbation theory. Calculations for GaSb, as given by (7) for the sections *A* and *B* in Fig. 3, are shown in Fig. 6(*a*). The solid line and the dotted line correspond to sections *A* and *B*, respectively. In both sections the dominant contrast variation is associated with the position of the $5\bar{1}\bar{1}$ line. This is in accordance with the general trend of the experimental observations (Fig. 1*b*), shown schematically in Fig. 3. It should be added that the profiles in Fig. 6(*a*) neglecting lines belonging to other zones than the [105] zone, also apply for the sections *C* and *D*, respectively.

Calculations have also been performed for the symmetrical sections *A'* and *B'* outside the 020 band.

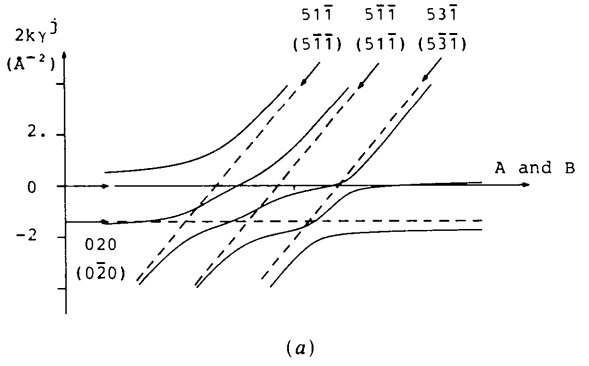

(*a*)

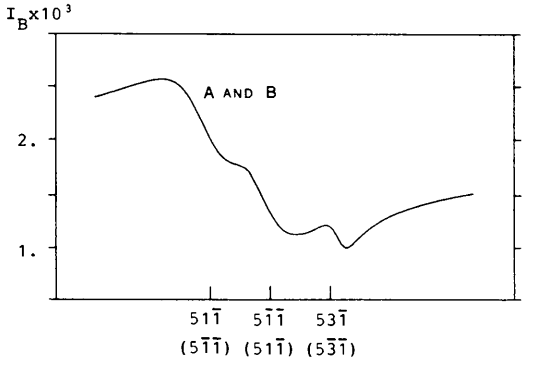

(*b*)

Fig. 4. (*a*) Calculated dispersion surface corresponding to sections *A* and *B* in Fig. 3 for GaSb. The indices in parentheses refer to section *B*. (*b*) Contrast profile for the sections *A* and *B* without *ij* coupling terms.

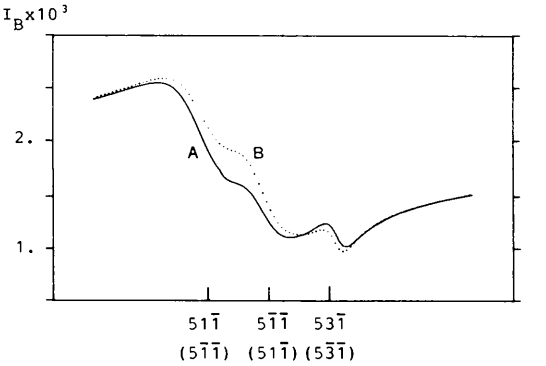

Fig. 5. Calculated contrast profiles corresponding to sections *A* and *B* in Fig. 3 for GaSb. Calculations without *ij* coupling terms, but using the eigenvectors obtained by solving the full non-Hermitian eigenvalue problem. Solid line, section *A*. Dotted line, section *B*. The indices in parentheses refer to section *B*.

These are six-beam calculations. The 040 and the $0\bar{4}0$ beams are added in the calculations for the sections A' and B', respectively. Like the intensity variations along the sections A and B, the contrast profiles along A' and B' should be similar according to standard theory. This is indeed not in agreement with the experiments (Fig. 1). The contrast profiles obtained with the present theory are shown in Fig. 6(b). For section A' (solid line) the most marked contrast fall may be associated with the position of the $53\bar{1}$ line. For section B' (dotted line) the contrast starts dropping markedly at the $5\bar{1}\bar{1}$ line position but does not reach a minimum until outside the $5\bar{3}\bar{1}$ line position. These results agree satisfactorily with the observations. Detailed features of the experimental observations which are inconsistent with these calculations may be ascribed to the limited number of beams taken into account. The good correspondence between Fig. 6 and the observed effects demonstrates that such effects may only be accounted for provided the ij coupling terms between the Bloch waves are included.

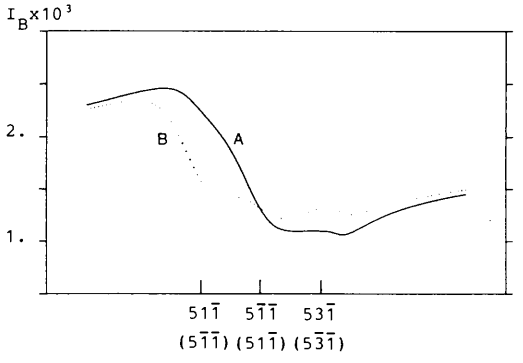

(a)

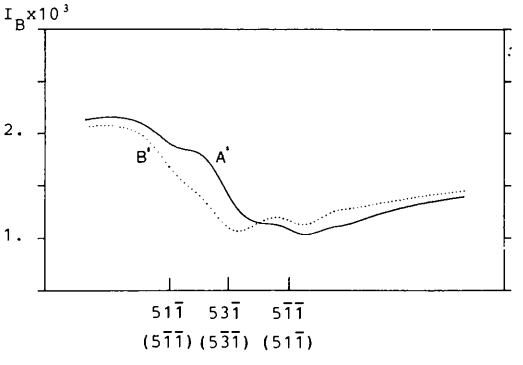

(b)

Fig. 6. Calculated contrast profiles for the sections A, A', B and B' in Fig. 3 for GaSb, including ij coupling terms. (a) Contrast profile, section A (solid line) and contrast profile, section B (dotted line). (b) Contrast profile, section A' (solid line) and contrast profile, section B' (dotted line). The indices in parentheses refer to sections B and B', respectively.

In the line pattern we have discussed for GaSb, the clue to the correct point-group determination is the absence of a mirror plane in the middle of the 020 band. Provided that only the zero-order Laue zone (ZOLZ) lines are important, the departure from centrosymmetry (or equivalently failure of Friedel's law) can, in principle, be detected in less-symmetric line patterns than the one shown in Fig. 3. Consider the hypothetical line pattern shown in Fig. 7. If only the ZOLZ lines indicated are taken into account, the eigenvalue matrices $\mathbf{M}$ [(9)] for sections A and B are related by $\mathbf{M}_A = \mathbf{M}_B^T$ and the dispersion surfaces are thus identical. For a centrosymmetric crystal the contrast profiles will hence be the same. However, differences such as the ones in Fig. 6 will be introduced for a non-centrosymmetric crystal. Absence of centrosymmetry can therefore, in principle, be determined. The practical use of such a procedure, however, is expected to be complicated by the influence of lines belonging to other zones since sections A and B, in general, will be affected differently. The possible observation of these kinds of effects depends on the many-beam interactions involved and to what extent the structure deviates from centrosymmetry. The latter point is exemplified in GaAs.

If we refer to the line pattern in Fig. 2, for GaAs, there was no experimental evidence of effects similar to those observed for GaSb. To see how this fits in with the theory, we have calculated the contrast profiles for sections A and B (Fig. 3) with and without the coupling terms, ij, between the different Bloch waves, from (7). The results are shown in Fig. 8. Fig. 8(a) refers to calculations without the coupling terms, ij, while the solid line and the dotted line in Fig. 8(b) correspond to sections A and B, respectively, including these coupling terms.

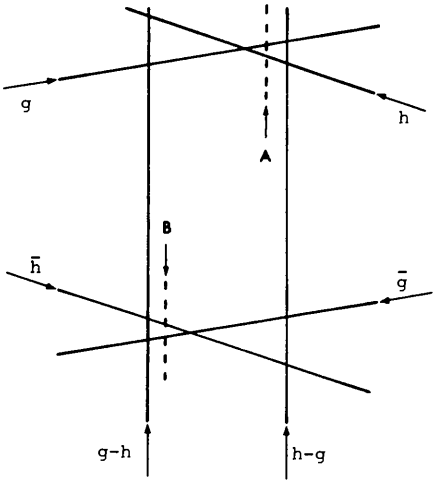

Fig. 7. A hypothetical line pattern showing sections A and B, having the same dispersion surface cut provided only lines belonging to the zero-order Laue zone are taken into account.

We notice first that, as for GaSb, the inclusion of the coupling terms between the different Bloch waves brings about corrections. The small fluctuations seen near both the intensity maximum and the intensity minimum in Fig. 8(*a*) are smoothed out in 8(*b*). However, when we compare the contrast profiles in (*b*), there are in this case, as opposed to the calculations for GaSb, only small differences. The most pronounced contrast variations are associated with the $5\bar{1}\bar{1}$ line in section *A* and the $51\bar{1}$ line in section *B*, giving almost identical profiles. This means that the calculations agree well with the experimental observations. The distinctions recognized between the profiles in Fig. 8(*b*) are too small to be seen in our experiments, which explains the erroneous identification of a mirror plane in the middle of the 020 band. The present calculations for GaAs also support our previous conclusions (Marthinsen & Høier, 1988) that the type of many-beam effects considered is rather insensitive to small deviations from centrosymmetry.

An interesting aspect of the effects discussed, which should be mentioned, relates to the dispersion surface. In recent studies on many-beam diffraction effects in channelling patterns it was concluded that the contrast effects could be interpreted from the dispersion surface and the contrast in a line was in most cases determined by a particular dispersion surface gap width (Marthinsen & Høier, 1986*b*; Marthinsen, 1986). The contrast effects investigated in this work, however, cannot be interpreted in this simple way. Firstly, the dispersion surfaces in question (*e.g.* Fig. 4*a*) are so complicated that the contrast in a particular line cannot be associated with a single gap at the dispersion surface. But the most important point is that the contrast effects we have discussed refer to differences along two sections with identical dispersion surfaces (for instance sections *A* and *B* in Fig. 3). These effects are thus of another kind than the non-systematic many-beam effects discussed previously, and, as demonstrated in the present work, they are due to interactions between the different backscattered Bloch waves. Only when such terms are present and non-negligible may the correct non-centrosymmetric point group be determined experimentally (Marthinsen & Høier, 1988).

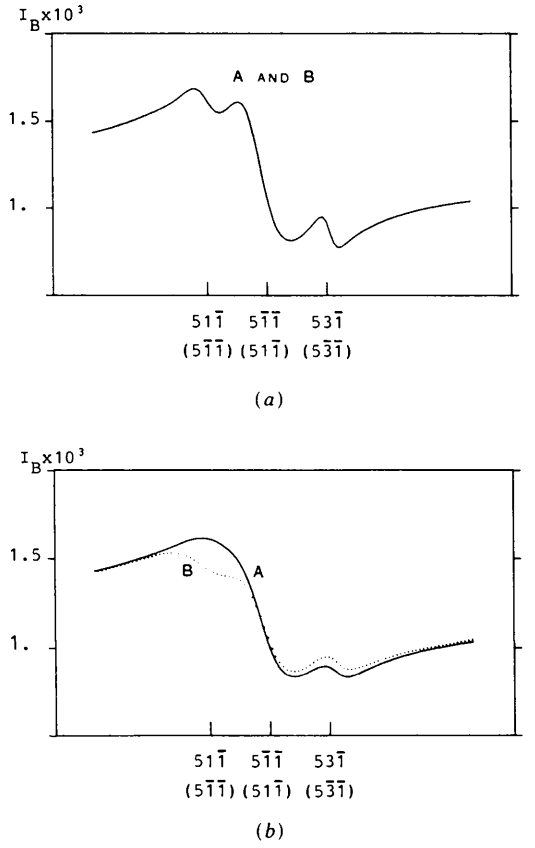

Fig. 8. Calculated contrast profiles corresponding to sections *A* and *B* in Fig. 3 for GaAs. (*a*) Contrast profile without *ij* coupling terms. (*b*) Contrast profile, section *A* (solid line) and contrast profile, section *B* (dotted line). The indices in parentheses refer to section *B*.

This work was supported in part by Norges Tekniske Høgskoles Fond. The electron channelling pattern in Fig. 2 was kindly supplied by Dr B. Tøtdal.

APPENDIX

The necessary modifications to the electron backscattering intensity expression upon the inclusion of absorption in the eigenvalue matrix [equation (9)] are discussed below. Numerical calculations are performed and compared for the sections *A* and *B* in GaSb (see Fig. 3).

It follows from standard dynamical electron diffraction theory (*e.g.* Humphreys, 1979) that the excitation coefficients c^i of the different Bloch waves in the crystal can be written $c^i = C_0^{i*}$ as assumed in the text [equation (1)]. However, when absorption is taken into account by adding a small imaginary term $iU'(\mathbf{r})$, the standard treatment no longer holds (David, Gevers & Stumpp, 1985). Since the non-Hermitian part of the potential is purely imaginary, we must have $U_g'^* = U'_{-g}$ and therefore for the complex potential

$$(U_g + iU'_g) \neq (U_{-g} + iU'_{-g})^*. \qquad (A1)$$

It hence follows that the eigenvalue matrix **M** [equation (9)] becomes a complex general matrix, and the eigenvectors of such a matrix do not form an orthonormal set. However, a generalized orthonormalization relation may be derived for this case. With some matrix algebra it is seen that

$$\langle C^i_{(2)} | C^j_{(1)} \rangle = \delta_{ij} \langle C^i_{(2)} | C^i_{(1)} \rangle \qquad (A2)$$

where the eigenvector $|C^j_{(1)}\rangle$ is a solution of the original eigenvalue equation [equation (9)], while $|C^i_{(2)}\rangle$ is a solution of the equation

$$\mathbf{M}^\dagger|C^i_{(2)}\rangle = 2k\gamma^{i\prime}|C^i_{(2)}\rangle \qquad (A3)$$

or equivalently

$$\langle C^i_{(2)}|\mathbf{M} = 2k\gamma^{i\prime *}\langle C^i_{(2)}| \qquad (A4)$$

where $\mathbf{M}^\dagger$ denotes the adjoint matrix of $\mathbf{M}$ and $\gamma^{i\prime *} = \gamma^i$.

Utilizing (A2), we obtain

$$c^i = \langle C^i_{(2)}|_0 / \langle C^i_{(2)}|C^i_{(1)}\rangle \qquad (A5)$$

where $\langle C^i_{(2)}|_0$ is the 0 component of the Bloch-wave eigenvector $\langle C^i_2|$.

By substituting such generalized excitation coefficients into the intensity expression [equation (7)] and neglecting the coupling terms, *ij*, the contrast profiles along sections *A* and *B* in Fig. 3 for GaSb have been calculated. The results are shown in Fig. 5.

References

DAVID, M., GEVERS, R. & STUMPP, H. (1985). *Acta Cryst.* A**41**, 204-206.

DOYLE, P. A. & TURNER, P. S. (1968). *Acta Cryst.* A**24**, 390-397.

FUJIMOTO, F. (1959). *J. Phys. Soc. Jpn*, **14**, 1558-1568.

GOODMAN, P. (1975). *Acta Cryst.* **31**, 804-810.

GOODMAN, P. & LEHMPFUHL, G. (1968). *Acta Cryst.* A**24**, 339-347.

GRADSHTEYN, I. S. & RYZHIK, I. M. (1980). *Tables of Integrals, Series and Products.* New York: Academic Press.

HALL, C. R. & HIRSCH, P. B. (1965). *Proc. R. Soc. London Ser. A*, **286**, 158-177.

HØIER, R. & MARTHINSEN, K. (1986). Proc. XIth Int. Congr. on Electron Microscopy, Kyoto, pp. 757-758.

HUMPHREYS, C. J. (1979). *Rep. Prog. Phys.* **42**, 1825-1887.

International Tables for X-ray Crystallography (1962). Vol. III. Birmingham: Kynoch Press. (Present distributor Kluwer Academic Publishers, Dordrecht.)

KOHRA, K. (1954). *J. Phys. Soc. Jpn*, **9**, 690-701.

MARTHINSEN, K. (1986). Dr. ing. thesis. Univ. of Trondheim-NTH, Norway.

MARTHINSEN, K., ANISDAHL, L. & HØIER, R. (1987). *Electron Microscopy and Analysis* 1987, edited by L. M. BROWN, pp. 143-146. Bristol: Institute of Physics.

MARTHINSEN, K. & HØIER, R. (1986*a*). Proc. XIth Int. Congr. on Electron Microscopy, Kyoto, Japan, pp. 759-760.

MARTHINSEN, K. & HØIER, R. (1986*b*). *Acta Cryst.* A**42**, 484-492.

MARTHINSEN, K. & HØIER, R. (1988). *Acta Cryst.* A**44**, 693-700.

MIYAKE, S. & UYEDA, R. (1950). *Acta Cryst.* **3**, 314.

MIYAKE, S. & UYEDA, R. (1955). *Acta Cryst.* **8**, 335-342.

PETERS, G. & WILKINSON, J. H. (1970). *Numer. Math.* **16**, 181-204.

REIMER, L., BADDE, H. G., SEIDEL, H. & BÜHRING, W. (1971). *Z. Angew. Phys.* **31**, 145-151.

SPENCER, J. P. & HUMPHREYS, C. J. (1980). *Philos. Mag.* A**42**, 433-451.

SPENCER, J. P., HUMPHREYS, C. J. & HIRSCH, P. B. (1972). *Philos. Mag.* **26**, 193-213.

STEEDS, J. W., TATLOCK, G. J. & HAMPSON, J. (1973). *Nature (London)*, **241**, 435-439.

STEEDS, J. W. & VINCENT, R. (1983). *J. Appl. Cryst.* **16**, 317-324.

THIESSEN, P. A. & MOLIÈRE, K. (1939). *Ann. Phys. (Leipzig)*, **34**, 449-460.

WILKINSON, J. H. & REINSCH, C. (1971). *Handbook of Automatic Computation.* Vol. II, *Linear Algebra.* Berlin: Springer-Verlag.

YAMAMOTO, T., MORI, M. & ISHIDA, Y. (1978). *Philos. Mag.* A**38**, 439-461.

Acta Cryst. (1988). A**44**, 707-714

Penrose Patterns and Related Structures. II. Decagonal Quasicrystals

BY AKIJI YAMAMOTO*

National Institute for Research in Inorganic Materials, Sakura-mura, Niihari-gun, Ibaraki 305, *Japan*

AND K. N. ISHIHARA

Department of Metal Science and Technology, Kyoto University, Sakyo-ku, Kyoto 606, *Japan*

(*Received* 27 *October* 1987; *accepted* 28 *April* 1988)

Abstract

Structural relations of the two decagonal phases in Al-Mn and Al-Fe alloys with the Penrose pattern are discussed based on structure-factor calculations and symmetry considerations. The electron diffraction patterns are explained by models with layer structures which consist of the stacking of four kinds of layers constructing the Penrose pattern. Al-Mn has six layers within a period along the tenfold axis while Al-Fe includes eight. A projection along the axis shows the Penrose pattern in both models. The symmetries of Al-Mn and Al-Fe are expressed by the five-dimensional superspace groups $P10_5/mmc$ and $P10_5mc$. These give the observed systematic extinction rules. In Al-Fe, an additional extinction rule due

* This work was performed partly while on leave as a visiting member of the Institute of Crystallography, University of Lausanne, Switzerland.

0108-7673/88/050707-08$03.00